Magnetization switching through spin-Hall-effect-induced chiral domain wall propagation

Guoqiang Yu,[*,†] Pramey Upadhyaya, Kin L. Wong, Wanjun Jiang, Juan G. Alzate, Jianshi Tang, Pedram Khalili Amiri,[*,‡] and Kang L. Wang[*,§]

Department of Electrical Engineering, University of California, Los Angeles, California 90095, USA

(Received 26 November 2013; revised manuscript received 11 February 2014; published 25 March 2014)

The influence of spin-Hall-effect spin torque (SHE-ST) induced by in-plane charge current was studied in microscale Ta/$Co_{20}Fe_{60}B_{20}$/TaO_x films with perpendicular magnetization. Simultaneous electrical transport and polar magneto-optical Kerr effect (MOKE) imaging experiments were used to investigate the switching dynamics. A rich set of switching behaviors was observed, which can be well understood by analyzing a switching-phase diagram and polar MOKE images, considering the competition between SHE-ST and the externally applied magnetic field. Furthermore, we found that domain walls with a particular chirality were dominant in our devices, which suggests the presence of the Dzyaloshinskii-Moriya interaction in the present material system.

DOI: 10.1103/PhysRevB.89.104421 PACS number(s): 75.76.+j

Electrical manipulation of magnetization using an in-plane charge current [1–6] has received growing attention in the spintronics community due to its potential applications in low-power nonvolatile memory and logic devices [7]. Spin-orbit torques such as those induced by the Rashba effect [8] and the spin-Hall effect (SHE) [9–14] have recently been utilized as the dominant mechanisms responsible for current-induced magnetization dynamics in such devices. In particular, it has been shown that the SHE generated by a heavy metal layer adjacent to a ferromagnetic thin film enables current-induced magnetization reversal at low switching current densities [1,2,4]. It can also be used to control domain wall (DW) motion in ferromagnetic nanowires with perpendicular magnetization [15,16], as well as to generate magnetization oscillations [3]. For the case of magnetization switching, three-terminal devices have been implemented, which use in-plane currents to write information into magnetic tunnel junctions, with tunnel magnetoresistance used for read-out [1,17]. This design separates the low-impedance writing process and the high-impedance sensing process [1], hence potentially offering a better energy-performance tradeoff compared to two-terminal magnetic tunnel junctions-based spintronic devices. For the case of DW devices, the SHE offers a new degree of freedom for controlling the DW motion by in-plane currents [15], enabling simpler and more flexible device designs for DW-based storage devices. In related experiments, it has also been reported recently that chiral DWs can be stabilized [16,18–20] as a result of the Dzyaloshinskii-Moriya interaction (DMI) [21,22] in (nonmagnetic metal)/(ferromagnetic metal)/(oxide) stack structures, where the inversion symmetry is absent along the growth direction. The combination of the SHE and DMI in such systems could have significant practical value for realizing fast DW motion in memory and logic devices [19]. Systematic study and understanding of the influence of the SHE on magnetization switching and chiral DW motion in perpendicularly magnetized systems is thus important to facilitate the potential applications of SHE-based devices.

In this report, SHE-induced magnetization switching dynamics are investigated in Ta/$Co_{20}Fe_{60}B_{20}$(CoFeB)/TaO_x trilayers with a perpendicular magnetic anisotropy. A rich set of switching behaviors was observed, which can be understood by constructing and analyzing a switching-phase diagram and polar magneto-optical Kerr effect (MOKE) images of the switching process. These complex switching phenomena are explained in terms of the competition between SHE spin torque (SHE-ST) and the externally applied magnetic field. Furthermore, our results indicate that DWs of a particular chirality (i.e., chiral DWs) can be stabilized in our structures, which suggests the presence of DMI in the present system.

Material stacks consisting of Ta(5)/$Co_{20}Fe_{60}B_{20}$ (1)/TaO_x layers (thickness in nanometers) were sputter-deposited at room temperature on a thermally oxidized Si/SiO_2 substrate. The TaO_x layer was formed by oxidizing a 1.5-nm Ta layer under an O_2/Ar plasma. The films were annealed at 200 °C for 30 min to improve crystallinity and to enhance the perpendicular magnetic anisotropy; they were subsequently patterned into 20 μm × 130 μm Hall bar devices by standard photolithography and dry-etching techniques. The device structure and measurement configuration are shown in Fig. 1(a), in which a dc current is applied along the x axis, and the voltage induced by the anomalous Hall effect (AHE) is measured along the y axis.

Figure 1(c) shows the anomalous Hall resistance (R_{AHE}) as a function of perpendicular magnetic field (H_z), which is measured at $I = +1$ mA. The square-shaped $R_{AHE}-H_z$ loop confirms the presence of perpendicular magnetic anisotropy. The anomalous Hall resistance is a proxy of magnetization in magnetic materials, which can thus be used to identify the direction of magnetization. For example, $M_z > 0$ ($M_z < 0$) results in $R_{AHE} < 0$ ($R_{AHE} > 0$), respectively, in our experiment. SHE-ST-induced magnetization switching is also shown in Figs. 1(d) and 1(e), in which both an electric current and an in-plane magnetic field are applied along the x axis. In the first case, $H_x > 0$, a positive current results in $M_z > 0$, while a negative current gives $M_z < 0$. In the second case, $H_x < 0$, the sign of the favored magnetization is reversed correspondingly. This behavior can be qualitatively explained by the symmetry breaking due to the application of an in-plane magnetic field [2,23]. With $H_x = +372$ Oe, the critical switching current is $I_{th} = 3$ mA, which is equivalent to a current density of 2.5×10^6 A/cm^2.

[*]Authors to whom correspondence should be addressed.
[†]Email address: guoqiangyu@ucla.edu
[‡]Email address: pedramk@ucla.edu
[§]Email address: wang@seas.ucla.edu

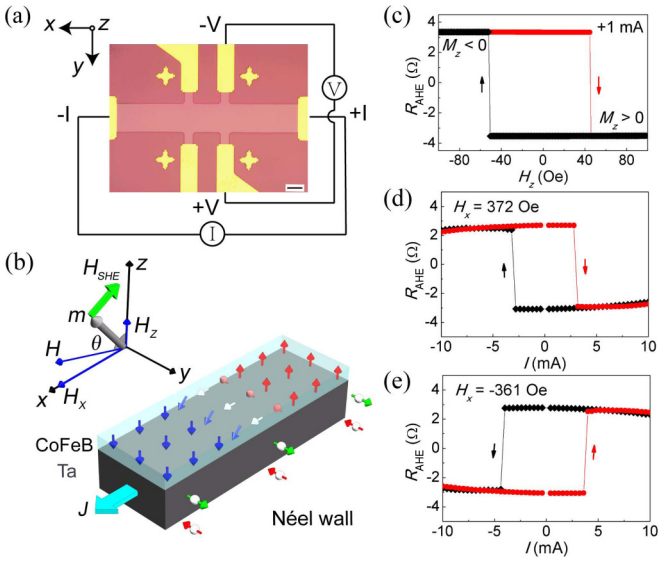

FIG. 1. (Color online) (a) Top view of the device consisting of a Ta/CoFeB/TaO_x stack structure (10 μm scale bar). (b) The effective field (H_{SHE}) acting on the magnetic moment, which is tilted away from the z axis in the xz plane by an external magnetic field. The field is in the xz plane, and the x and z components are also shown. Schematic of the spin texture inside a NW is shown as well. Red, blue and white arrows present the magnetization pointing up, pointing down, and in the DW, respectively. Green and red arrows on the side wall show the directions of the spin polarized electrons. (c) Dependence of anomalous Hall resistance on the perpendicular magnetic field H_z measured at a positive current of +1 mA. (d), (e) Current-induced switching at room temperature in the presence of a constant in-plane magnetic field H_x, with (d) $H_x = 372$ Oe and (e) $H_x = -361$ Oe.

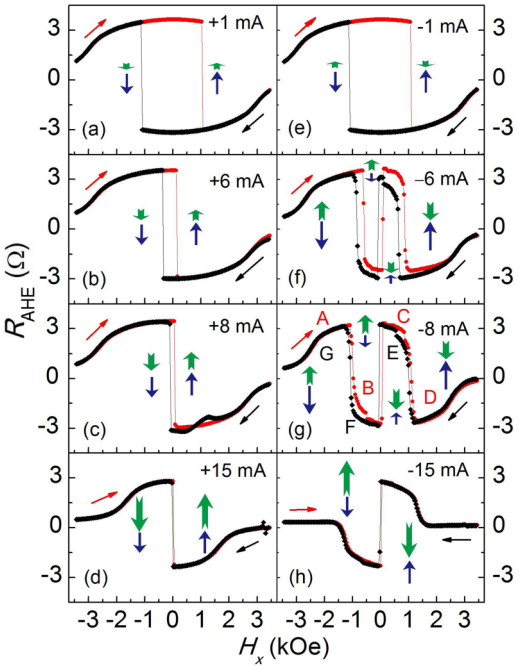

FIG. 2. (Color online) AnomalousHall resistance as a function of x-component field H_x at $I_x = \pm 1$ mA, ± 6 mA, ± 8, and ± 15 mA. The external magnetic is $\vec{H} = H_x\hat{x} + H_z\hat{z}$, at the polar angle of $\theta \sim 88°$. The left (right) figures show the change of hysteresis loops when increasing current of positive (negative) values. The red (black) curve corresponds to the magnetic field sweeping forward (backward). A–G in (g) labels the magnetic field values, where polar MOKE images are taken for illustrating the multiple switching due to the competition between H_z and SHE (in the z-axis direction), as shown in Fig. 4. The red (black) labels correspond to the magnetic field sweeping forward (backward). The competition is schematically shown by blue (H_z) and green (SHE) arrows, where the length of the arrows represents the strength of field.

The influence of SHE-ST on the magnetization is first studied by sweeping the external magnetic field in the presence of various constant in-plane currents. An applied magnetic field is applied in the xz plane ($\vec{H} = H_x\hat{x} + H_z\hat{z}$) with a very small tilting angle away from the x axis. The polar angle θ is ~88°, as shown in Fig. 1(b). The in-plane component of the magnetic field (H_x) tilts the magnetization slightly away from its easy axis. The nonzero H_z is applied simultaneously to ensure the perpendicular magnetization switching. It is noted that only H_x is measured, and the H_z is estimated as $H_x\cot(\theta)$. Figures 2(a)–2(h) show the R_{AHE} as a function of the tilted magnetic field for various positive and negative currents.

When $I = \pm 1$ mA, switching fields are at $H_x \sim \pm 1.1$ kOe, as shown in Figs. 2(a) and 2(e). When H_x is positive, $M_z > 0$, as suggested by the negative R_{AHE} values (the direction of M_z is determined by the sign of H_z). It is noted that no clear difference between the two R_{AHE}-H_x loops for $I = \pm 1$ mA is observed. When $I > +15$ mA and $I < -15$ mA, however, the switching fields are reduced significantly [see Figs. 2(d) and 2(h)]. For $I > +15$ mA, the positive H_x (i.e., also positive H_z for $\theta \sim 88°$) favors $M_z > 0$, and the negative H_x (i.e., also negative H_z) yields $M_z < 0$. By contrast, for $I < -15$ mA, positive H_x gives $M_z < 0$, and the negative H_x favors $M_z > 0$, as shown in Fig. 2(h). These results indicate that the SHE-ST dominates the favored magnetization direction when the applied current is large. It is interesting to note that multiple switching events occur for the intermediate currents (-8 mA $< I < -6$ mA), as shown in Figs. 2(f) and 2(g). To the best of our knowledge, this behavior has not yet been reported for SHE-ST-induced switching. Moreover, the presence of such multiple switching depends on the direction of the applied current, as evident from a comparison to Figs. 2(b) and 2(c).

To understand the reason for this behavior, we construct a switching-phase diagram in a similar fashion (described in Ref. [2]), which is depicted in Fig. 3. This diagram contains five different regions and was constructed based on a series of current-induced switching experiments for magnetic fields applied to the device at different angles θ (88° to 91°). The switching-phase diagram is approximately symmetric for $\theta \sim 90°$, a behavior that has been previously explained using a zero-temperature macrospin model [2]. In regions I and IV, $M_z < 0$ is favored, while in regions II and III, $M_z > 0$ is preferred. Region V is a bistable region where both $M_z < 0$ and $M_z > 0$ are allowed, depending on the history of applied fields and currents. The phase boundaries shift to the left for $\theta \sim 88°$ and $\theta \sim 89°$ and to the right for $\theta \sim 91°$. This effect is more pronounced for higher magnetic fields and higher a value of θ.

This experimental switching-phase diagram can be used to explain the multiple switching events observed in Fig. 2. For

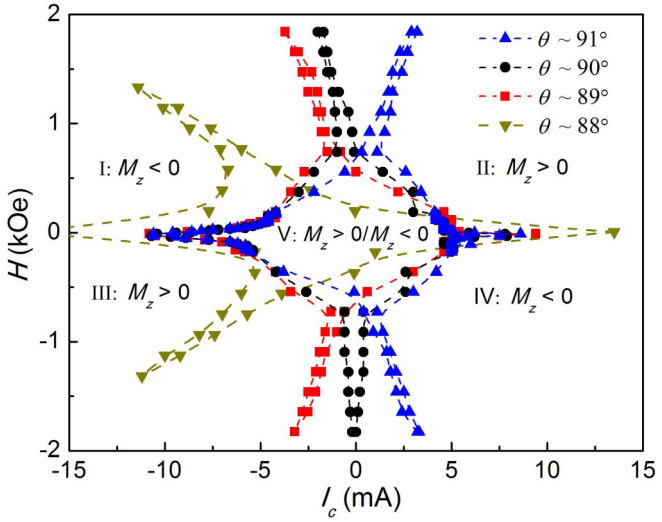

FIG. 3. (Color online) Experimentally determined switching-phase diagram with the externally applied field $\vec{H}$ at angles of $\theta \sim 91°$, $\theta \sim 90°$, $\theta \sim 89°$, and $\theta \sim 88°$. For each value of applied field, corresponding switching currents (I_c) are obtained by sweeping current. For each value of θ, the area is divided into five regions, represented by I–V. The magnetizations in these five regions are $M_z < 0$, $M_z > 0$, $M_z > 0$, $M_z < 0$, and bistable ($M_z > 0$ or $M_z < 0$), respectively.

example, when $\theta \sim 88°$ and $I > 0$, the magnetic field sweep in the switching-phase diagram remains in regions II, IV, and V of the phase diagram; hence, only one switching event is observed as the field is swept in a particular direction. When $\theta \sim 88°$ and $I < 0$, on the other hand, when the current density reaches a threshold value (which depends on the applied filed angle), the magnetic field sweep passes through all the regions IV, III, V, I, and II. As a result, multiple switching events occur as the field is swept in a particular direction, corresponding to the favored magnetization orientations in different regions. Similarly, at $\theta > 90°$, the multiple switching events are observed for positive currents only (see Supplemental Material in Ref. [24]).

The angle dependence of the switching-phase diagram strongly suggests the important contribution from H_z, which can be analyzed by considering the effective field induced by the SHE-ST, which acts on the magnetization vector [25] and is given by

$$\vec{H}_{\mathrm{SHE}} = -\tau_{\parallel}^{\mathrm{SHE}}(\hat{m} \times (\hat{z} \times \hat{j})). \quad (1)$$

Here, $\hat{m}$, $\hat{z}$, and $\hat{j}$ are the unit vectors along the direction of magnetization [see Fig. 1(b)], the z axis, and the current flow, respectively. The magnitude of SHE-ST $\tau_{\parallel}^{\mathrm{SHE}}$ can be written as $\tau_{\parallel}^{\mathrm{SHE}} = \frac{\hbar\theta_{\mathrm{SHE}}J}{2|e|M_s t_F}$, where M_s is the saturation magnetization (which is measured to be ~700 emu/cc), t_F is the thickness of the ferromagnetic layer, e is the electron charge, $\hbar$ is the reduced Planck constant, θ_{SHE} is the spin-Hall angle, and J is the electrical current density. It is noted that θ_{SHE} has previously been reported to be between -0.12 and -0.15 under this convention [1,16,26]. The spin-Hall angle was also measured to be $\theta_{\mathrm{SHE}} = -0.05$ in our samples using a vector measurement method [26,27].

For the geometry of our experiments, $\hat{j}$ is aligned with $\hat{x}$, and $\hat{m}$ is tilted away from the z axis by H_x, as shown in Fig. 1(b). Based on equation (1), the direction of $\vec{H}_{\mathrm{SHE}}$ in the z axis can be expressed as $\vec{n}_{H_{\mathrm{SHE}}^z} = \frac{H_x J_x}{|H_x||J_x|}\hat{z}$, which is related to both the directions of H_x and J_x. When $\theta \sim 88°$ and $J_x > 0$, $\vec{n}_{H_{\mathrm{SHE}}^z}$ follows the direction of $\vec{H}_Z$, which is one of the reasons for the reduction of coercivity [see Figs. 2(a)–2(d)] when the bias current is increased. However, when $J_x < 0$, $\vec{n}_{H_{\mathrm{SHE}}^z}$ is opposite to $\vec{H}_Z$. Specifically, at large negative magnetic fields [point A in Fig. 2(g)], $\vec{H}_Z$ determines the direction of the magnetization, and the magnetization configuration lies in area IV of the phase diagram in Fig. 3 ($M_z < 0$). The favored direction of magnetization and strength of $\vec{H}_Z$(Blue wide arrows) and SHE-ST (green wide arrows) are also schematically shown in the Figs. 2(a)–2(h). As $|\vec{H}_Z|$ decreases and $|\vec{H}_{\mathrm{SHE}}^z| > |\vec{H}_Z| + H_c$, the magnetization is reversed by the current-induced $\vec{H}_{\mathrm{SHE}}^z$, and the system thus enters into region III from region IV(point B). Here, $\vec{H}_{\mathrm{SHE}}^z$ represents the effective field due to SHE-ST along the z axis, and H_c is the effective coercive field. By reducing the external field to zero and subsequently changing its direction, the direction of $\vec{H}_{\mathrm{SHE}}^z$ is reversed due to the different direction of $\hat{m}$. The reversed $\vec{H}_{\mathrm{SHE}}^z$ results in magnetization switching while entering region I [point C in Fig. 2(g). When the positive magnetic field is larger than $|\vec{H}_{\mathrm{SHE}}^z| + H_c$, another switching event occurs, and the switching-phase diagram eventually enters region II [point D in Fig. 2(g)], which is where the positive applied field dominates the switching behavior. Thus, the multiple switching events can be well explained as a result of the competition between SHE-ST and the external magnetic field, $\vec{H}_Z$.

To further understand the switching mechanism and the observed multiple switching events, we performed polar MOKE imaging on the Hall bar by using a space-resolved (360-nm resolution) and time-resolved (20-ms resolution) polar MOKE microscope [28,29]. Figure 4 shows the magnetization configurations at different external magnetic fields that correspond to points A–G, as labeled in Fig. 2(g). Here, the red (blue) color represents $M_z > 0$ ($M_z < 0$), respectively. The polar MOKE images shown in Fig. 4 clearly suggest that the switching takes place through DW propagation. For example, between points A and B, the switching is realized by nucleating a DW of the left side of the Hall bar, which subsequently moves from left to right. At point B, the magnetization in the Hall bar channel is fully reserved. It is noted that the magnetizations in the four electrodes are not yet reversed, which can be attributed to a lower current density (and hence a smaller amplitude of SHE-ST) compared to that in the Hall bar channel. The switching events from B to C, D to E, and E to F are all similar, and the SHE-ST dominates the switching in these cases (given that $|\vec{H}_{\mathrm{SHE}}^z| > |\vec{H}_Z| + H_c$). However, the other switching events (from point C to D and F to G) can be attributed to field-driven switching since $|\vec{H}_Z| > |\vec{H}_{\mathrm{SHE}}^z| + H_c$. It is noted that the DW motion starts from the Hall bar electrode area, in this case due to the presence of the DW there, as shown in Fig. 4, which is different from the current-induced switching.

In the current-induced switching ($|\vec{H}_{\mathrm{SHE}}^z| > |\vec{H}_Z| + H_c$), the observed DW motion could have two contributions: (i)

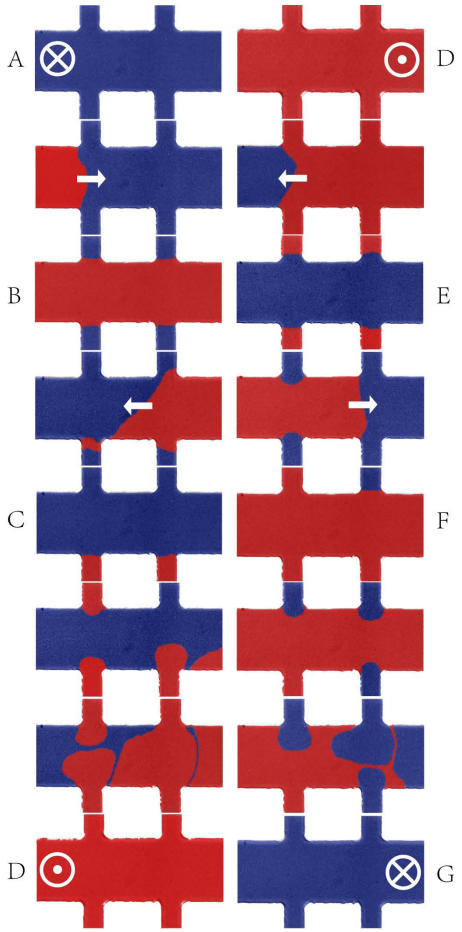

FIG. 4. (Color online) MOKE images at different H_x points (A→D→G), shown in Fig. 2(g) with $I_x = -8$ mA. The red (blue) color shows the up (down) magnetization, which is also labeled by white marks (see Fig. 1). The white arrows in the figures indicate the magnetization direction in the DW, which is considered to approximately follow the direction of H_x. The white ⊙ and ⊗ present the magnetization direction in the magnetic domains.

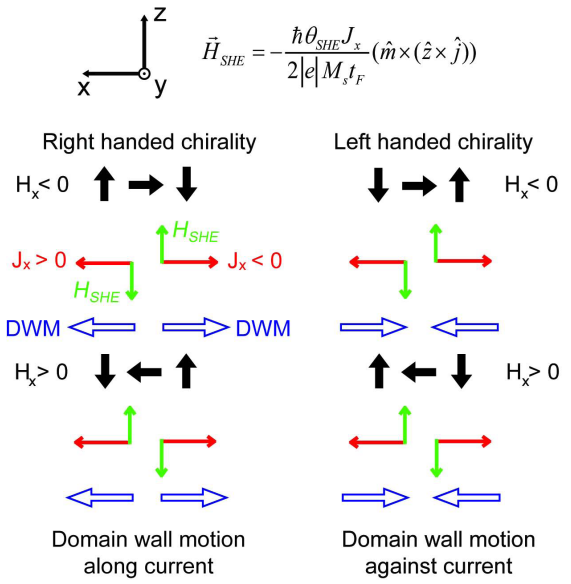

FIG. 5. (Color online) Schematic representation of the domain wall (DW) motion induced by SHE-ST for both right- and left-handed chiral DWs. The formula represents the effective field (H_{SHE}) induced by SHE. The black arrows indicate the magnetizations in chiral DW. The direction of magnetization in the center of DW is consistent with the external field (H_x). The directions of H_{SHE} corresponding to different DW structure and J_x directions are shown by the green and red marks. The left (right) side magnetic configuration corresponds to right- (left-)handed chirality, where the DW moves along (against) the current direction.

a conventional spin transfer torque (STT) due to angular momentum transfer via current flowing through the CoFeB layer, in which the direction of DW motion is opposite to the current flow direction [30], and (ii) SHE-ST-induced DW motion that is caused by currents flowing in the heavy metal underlayer [15,16]. In our case, the observed direction of DW motion is in the same direction as the current flow, which thus allows us to exclude the contribution from conventional STT in CoFeB layer, indicating a predominantly SHE-ST-induced motion.

As the effective field on the magnetization in the Néel walls (NWs) is out-of-plane, we can compare $|\vec{H}^z_{\mathrm{SHE}}|$ and $|\vec{H}_Z| + H_c$ values in our devices. Here we consider the magnetization in the NW to be approximately along the x axis, while noting that, in principle, nonzero Rashba-like fields and the wall demagnetization energy would tend to orient the magnetization away from the x axis. Hence, while a quantitative analysis requires knowledge of the detailed magnetization angle across the DW, an approximate comparison of these fields can nonetheless be performed. The value of $|\vec{H}^z_{\mathrm{SHE}}|$ can be calculated to be 16.7 Oe at the current value of −8 mA, based on equation (1). As shown in Fig. 2(g), in the case of −8 mA current, the competition occurs in the broad range of 84 to 1182 Oe for positive applied magnetic fields. As the tilt angle is ∼2°, $|\vec{H}_Z|$ can be calculated to be in the range of 2.9 to 41.5 Oe. The coercive field H_c can be approximately ignored due to thermal effects, since there is nearly no hysteresis in the competition region. In this case, $|\vec{H}^z_{\mathrm{SHE}}|$ and $|\vec{H}_Z|$ are thus generally comparable, which qualitatively confirms the understanding based on the competition of these fields, as presented above.

In addition, an important consequence of SHE-ST-induced DW motion is that the direction of DW motion is determined solely by the chirality of the DW [16] for a material with a given sign of spin-Hall angle, as illustrated in Fig. 5. In the current system, the direction of DW motion is always along the current flow when the switching is current-induced, which indicates that DWs of right-handed chirality are favored. In the following, we focus on the discussion of chirality for the cases of current-induced switching (A to B, B to C, D to E, and E to F). The magnetizations in the DW can be approximately considered to follow the direction of H_x, as indicated by white arrows in Fig. 4. This is due to the fact that NWs can be stabilized by applying a magnetic field along the wire [15], with center magnetization vectors in the NWs pointing along the field direction. Thus, by analyzing polar MOKE images of the switching events, the chirality of the DWs can be inferred.

For magnetization switching from A to B in Fig. 4, a DW is first nucleated at the left side of the Hall bar, which subsequently moves to the right side. During the DW motion, the magnetization in the Hall bar (from left

to right) is thus pointing up, pointing right, and pointing down (up-right-down), respectively. The chirality of the DW can thus be identified [18] to be right-handed, as shown in Fig. 5. For the switching from point B to C, a DW is also first nucleated at the left side of the device. During the DW motion, the magnetization in the Hall bar is pointing down, pointing left, and pointing up (down-left-up), which also follows a right-handed chirality, as shown in Fig. 5. The cases of D to E and E to F switching follow similarly. Here the magnetization directions are down-left-up and up-right-down, respectively, again following a right-handed chirality. Hence, only right-handed chirality was observed in our experiments for $|\vec{H}^z_{\rm SHE}| > |\vec{H}_Z| + H_c$. Similar results were observed in three other Hall bar devices in the same batch of samples measured for verification of the results.

The observation of only one chirality in our experiments is significant because in general, both chiralities of the NWs, i.e., right-handed (up-right-down) and left-handed (down-right-up), should exist and could result in the switching between points A and B, where $H_x > 0$. In this case, switching via the right-handed DW configuration occurs by the DW nucleation at the left side of the Hall bar, while switching via the left-handed configuration could, in principle, occur by the DW nucleation on the right side of the Hall bar. As shown in Fig. 5, for right-handed chiral DWs, the motion is along the current flow, while it is opposite to the current flow for left-handed chiral DWs. Thus, both chiral DWs would, in principle, result in the switching of the magnetization from $M_z < 0$ to $M_z > 0$. However, we only observed the right-handed chiral nucleation from MOKE experiments.

To exclude the possible contribution from structural asymmetry (i.e., giving rise to asymmetry of nucleation energies between the left and right sides of the sample), we also imaged the multiple switching events for the case of +8 mA current with $\theta > 90°$ (see Supplemental Material in Ref. [24]). In the cases of $|\vec{H}^z_{\rm SHE}| > |\vec{H}_Z| + H_c$, the DWs are always first nucleated at the right side of the Hall bar and thus only the right-handed chiral nucleation was observed, which consequently excludes the contribution from structural asymmetries. This behavior suggests the presence of the DMI in our system, affecting the chirality of the DWs, as discussed below.

The DMI is believed to play a crucial role in determining the chirality of DWs in systems that lack inversion symmetry [18,31–34]. The energy of DMI can be expressed as $E_{\rm DM} = \boldsymbol{D}_{ij} \cdot (\boldsymbol{S}_i \times \boldsymbol{S}_j)$, where $\boldsymbol{D}_{ij}$ is the DMI vector [18], and $\boldsymbol{S}_i$ and $\boldsymbol{S}_j$ are spin vectors located on neighboring atomic sites i and j. The $\boldsymbol{D}_{ij}$ vector lies in the film plane and is perpendicular to the spin-spiral direction, i.e., perpendicular to the position vector connecting the neighboring spins [22,31]. In a NW, $\boldsymbol{S}_i \times \boldsymbol{S}_j$ is nonzero, and its direction is parallel to the direction of $\boldsymbol{D}_{ij}$. Thus the sign of $E_{\rm DM}$ in the NW is determined by the direction of $\boldsymbol{D}_{ij}$ and the chirality of the NW. The energy is lower for one chirality, while the energy is increased by $2E_{\rm DM}$ for the opposite chirality, resulting in one type of chirality being energetically preferred. This is the origin of the preferred right-handed chirality of the NWs in our samples. It has been previously reported that NWs with a left-handed chirality are preferred in both Pt/CoFe/MgO and Ta/CoFe/MgO structures by S. Emori *et al.* [16]. However, our results show an opposite chirality in the present Ta/CoFeB/TaO_x system, which clearly requires further studies.

In summary, we have studied the SHE-induced switching of magnetization via DW motion in Ta/CoFeB/TaO_x structures through simultaneous electrical transport and polar MOKE imaging measurements. The presence of multiple switching events was observed and explained as a result of the competition between SHE-ST and the externally applied magnetic field (H_z). In addition, only right-handed chiral DW nucleation is observed in the process of current-induced switching. Our results strongly indicate the presence of a DMI effect in our samples, which leads to a lower nucleation energy for right-handed chiral DWs in the device.

ACKNOWLEDGMENTS

This work was partially supported by the Defense Advanced Research Projects Agency (DARPA) program on Nonvolatile Logic (NVL) and by the National Science Foundation (NSF) Nanosystems Engineering Research Center for Translational Applications of Nanoscale Multiferroic Systems (TANMS). This work was also supported in part by the Function Accelerated nanoMaterial Engineering (FAME) Center, one of six centers of the Semiconductor Technology Advanced Research network (STARnet), a Semiconductor Research Corporation (SRC) program sponsored by Microelectronics Advanced Research Corporation (MARCO) and DARPA.

[1] L. Q. Liu, C. F. Pai, Y. Li, H. W. Tseng, D. C. Ralph, and R. A. Buhrman, Science **336**, 555 (2012).
[2] L. Q. Liu, O. J. Lee, T. J. Gudmundsen, D. C. Ralph, and R. A. Buhrman, Phys. Rev. Lett. **109**, 096602 (2012).
[3] L. Q. Liu, C. F. Pai, D. C. Ralph, and R. A. Buhrman, Phys. Rev. Lett. **109**, 186602 (2012).
[4] C. F. Pai, L. Q. Liu, Y. Li, H. W. Tseng, D. C. Ralph, and R. A. Buhrman, Appl. Phys. Lett. **101**, 122404 (2012).
[5] I. M. Miron, G. Gaudin, S. Auffret, B. Rodmacq, A. Schuhl, S. Pizzini, J. Vogel, and P. Gambardella, Nature Materials **9**, 230 (2010).
[6] I. M. Miron, K. Garello, G. Gaudin, P.-J. Zermatten, M. V. Costache, S. Auffret, S. Bandiera, B. Rodmacq, A. Schuhl, and P. Gambardella, Nature (London) **476**, 189 (2011).
[7] K. L. Wang, J. G. Alzate, and P. K. Amiri, J. Phys. D **46**, 074003 (2013).
[8] Yu. A. Bychkov and E. I. Rashba, Pis'ma Zh. Eksp. Teor. Fiz. **39**, 66 (1984) [JETP Lett. **39**, 78 (1984)].
[9] M. I. Dyakonov and V. I. Perel, Phys. Lett. A **35**, 459 (1971).
[10] J. E. Hirsch, Phys. Rev. Lett. **83**, 1834 (1999).
[11] S. F. Zhang, Phys. Rev. Lett. **85**, 393 (2000).
[12] J. Sinova, D. Culcer, Q. Niu, N. A. Sinitsyn, T. Jungwirth, and A. H. MacDonald, Phys. Rev. Lett. **92**, 126603 (2004).
[13] Y. K. Kato, R. C. Myers, A. C. Gossard, and D. D. Awschalom, Science **306**, 1910 (2004).
[14] S. O. Valenzuela and M. Tinkham, Nature **442**, 176 (2006).
[15] P. P. J. Haazen, E. Murè, J. H. Franken, R. Lavrijsen, H. J. M. Swagten, and B. Koopmans, Nat Mater **12**, 299 (2013).

[16] S. Emori, U. Bauer, S. M. Ahn, E. Martinez, and G. S. D. Beach, Nat. Mater. **12**, 611 (2013).
[17] M. Yamanouchi, L. Chen, J. Kim, M. Hayashi, H. Sato, S. Fukami, S. Ikeda, F. Matsukura, and H. Ohno, Appl. Phys. Lett. **102**, 212408 (2013).
[18] M. Heide, G. Bihlmayer, and S. Blügel, Phys. Rev. B **78**, 140403 (2008).
[19] A. Thiaville, S. Rohart, E. Jue, V. Cros, and A. Fert, Europhys. Lett **100**, 57002 (2012).
[20] K. S. Ryu, L. Thomas, S. H. Yang, and S. Parkin, Nature Nanotechnology **8**, 527 (2013).
[21] I. E. Dzyaloshinskii, Sov. Phys. JETP **5**, 1259 (1957).
[22] T. Moriya, Phys. Rev. **120**, 91 (1960).
[23] G. Q. Yu, P. Upadhyaya, Y. Fan, J. G. Alzate, W. Jiang, K. L. Wong, S. Takei, S. A. Bender, M. Lang, J. Tang, Y. Tserkovnyak, P. K. Amiri, and K. L. Wang, arXiv:1311.0929 (2013).
[24] See Supplemental Material at http://link.aps.org/supplemental/10.1103/PhysRevB.89.104421 for MOKE images of the multiple switching events for the case of $+8$ mA current with $\theta > 90°$.
[25] A. V. Khvalkovskiy, V. Cros, D. Apalkov, V. Nikitin, M. Krounbi, K. A. Zvezdin, A. Anane, J. Grollier, and A. Fert, Phys. Rev. B **87**, 020402 (2013).
[26] J. Kim, J. Sinha, M. Hayashi, M. Yamanouchi, S. Fukami, T. Suzuki, S. Mitani, and H. Ohno, Nature Materials **12**, 240 (2013).
[27] U. H. Pi, K. W. Kim, J. Y. Bae, S. C. Lee, Y. J. Cho, K. S. Kim, and S. Seo, Appl. Phys. Lett. **97**, 162507 (2010).
[28] W. Jiang, P. Upadhyaya, Y. Fan, J. Zhao, M. Wang, L.-T. Chang, M. Lang, K. L. Wong, M. Lewis, Y.-T. Lin, J. Tang, S. Cherepov, X. Zhou, Y. Tserkovnyak, R. N. Schwartz, and K. L. Wang, Phys. Rev. Lett. **110**, 177202 (2013).
[29] W. Jiang, Y. Fan, P. Upadhyaya, M. Lang, M. Wang, L.-T. Chang, K. L. Wong, J. Tang, M. Lewis, J. Zhao, L. He, X. Kou, C. Zeng, X. Z. Zhou, R. N. Schwartz, and Kang L. Wang, Phys. Rev. B **87**, 014427 (2013).
[30] S. S. P. Parkin, M. Hayashi, and L. Thomas, Science **320**, 190 (2008).
[31] G. Chen, J. Zhu, A. Quesada, J. Li, A. T. N'Diaye, Y. Huo, T. P. Ma, Y. Chen, H. Y. Kwon, C. Won, Z. Q. Qiu, A. K. Schmid, and Y. Z. Wu, Phys. Rev. Lett. **110**, 177204 (2013).
[32] M. Bode, M. Heide, K. von Bergmann, P. Ferriani, S. Heinze, G. Bihlmayer, A. Kubetzka, O. Pietzsch, S. Blügel, and R. Wiesendanger, Nature **447**, 190 (2007).
[33] S. Heinze, K. von Bergmann, M. Menzel, J. Brede, A. Kubetzka, R. Wiesendanger, G. Bihlmayer, and S. Blugel, Nature Physics **7**, 713 (2011).
[34] P. Ferriani, K. von Bergmann, E. Y. Vedmedenko, S. Heinze, M. Bode, M. Heide, G. Bihlmayer, S. Blugel, and R. Wiesendanger, Phys. Rev. Lett. **101**, 027201 (2008).